

Reaction of carbon monoxide and hydrogen on neutral Nb₈ clusters in the gas phase

Y. Xie and S.-G. HeF. Dong and E. R. Bernstein

Citation: *The Journal of Chemical Physics* **128**, 044306 (2008); doi: 10.1063/1.2813348

View online: <http://dx.doi.org/10.1063/1.2813348>

View Table of Contents: <http://aip.scitation.org/toc/jcp/128/4>

Published by the *American Institute of Physics*

COMPLETELY

REDESIGNED!



**PHYSICS
TODAY**

Physics Today Buyer's Guide
Search with a purpose.

Reaction of carbon monoxide and hydrogen on neutral Nb₈ clusters in the gas phase

Y. Xie and S.-G. He

Department of Chemistry, Colorado State University, Fort Collins, Colorado 80523-1872, USA

F. Dong and E. R. Bernstein^{a)}

Department of Chemistry and NSF ERC for Extreme Ultraviolet Science and Technology, Colorado State University, Fort Collins, Colorado 80523-1872, USA

(Received 28 November 2006; accepted 24 October 2007; published online 25 January 2008)

Reactions of neutral V_n, Nb_n, and Ta_n metal clusters ($n \leq 11$) with CO+H₂ mixed gases and CH₃OH in a flow tube reactor (1–50 Torr) are studied by time of flight mass spectroscopy and density functional theory calculations. Metal clusters are generated by laser ablation, and reactants and products are ionized by low fluence ($\sim 200 \mu\text{J}/\text{cm}^2$) 193 nm excimer laser light. Nb_n clusters exhibit strong size dependent reactivity in reactions both with CO+H₂ and CH₃OH compared with V_n and Ta_n clusters. A “magic number” (relatively intense) mass peak at Nb₈COH₄ is observed in the reaction of Nb_n clusters with CO+H₂, and CH₃OH is suggested to be formed. This feature at Nb₈COH₄ remains the most intense peak independent of the relative concentrations of CO and H₂ in the flow tube reactor. No other Nb_n, Ta_n, or V_n feature behaves in this manner. In reactions of CH₃OH with metal clusters M_n (M=V, Nb, and Ta, $n=3-11$), nondehydrogenated products M_nCOH₄/M_nCH₃OH are only observed on Nb₈ and Nb₁₀, whereas dehydrogenated products M_nCO/CM_nO are observed for all other clusters. These observations support the suggestion that CH₃OH can be formed on Nb₈ in the reaction of Nb_n with CO+H₂. A reaction mechanism is suggested based on the experimental results and theoretical calculations of this work and of those in the literature. Methanol formation from CO+H₂ on Nb₈ is overall barrierless and thermodynamically and kinetically favorable. © 2008 American Institute of Physics.

[DOI: 10.1063/1.2813348]

I. INTRODUCTION

Methanol synthesis from carbon monoxide and hydrogen,



is an important industrial process, and it offers a clear economic and political advantage compared with oil refining.¹ Methanol is not only an essentially fundamental feedstock for the chemical industry but it is also a clean liquid fuel and can be utilized in automobiles and other (e.g., fuel cell) applications.^{2–4} The syngas (CO+H₂) catalytic reaction to produce CH₃OH has attracted deep interest for nearly a century.^{5,6} Most catalysis studies are focused on condensed phase reactions, but a few studies are done with gas phase systems.^{7–9} Clusters are good models to simulate active sites of complex solid state catalysts. Molecular level mechanisms for condensed phase catalytic reactions may be understood through the study of gas phase model reactions. Moreover, theoretical calculations can be used to help us in the interpretation of experimental results and the prediction of detailed reaction mechanisms for finite cluster systems.

A number of studies have been carried out for the reaction of M_n (M=V and Nb) with CO and H₂, and a brief review for these systems is given below. Neutral transition

metal clusters (M_n) are typically generated by laser ablation of the metal¹⁰ and two different apparatuses are employed to investigate their reactivity. One is called a fast flow or flow tube reactor,^{11–14} and the other is called a pickup cell.^{15–19}

The major difference between the two cells is that seeded reactant gas (A, B, etc.) in a large amount of inert buffer gas ($\sim 1-50$ Torr) is used in the flow tube reactor, while low pressure (~ 1 mTorr) pure reactant gas is used in the pickup cell. As a result, collision intermediates (M_nA) can be stabilized by the buffer gas in the flow tube reactor and reactant species can be additionally cooled. There is no buffer gas to stabilize the intermediates in the pickup cell so M_nA either directly dissociates (M_n+A), undergoes further reactive dissociation (C+D, C and D ≠ A), or is detected in a metastable state.²⁰ Consequently, the chemistry in a pickup cell occurs at a much higher temperature ($T \sim 700$ K) than that in a flow tube reactor ($T \sim 300$ K).

Reactions of neutral Nb_n clusters with CO and D₂ in a flow tube reactor have been reported by Morse *et al.*,²¹ Kaldor and co-workers,^{22,23} and Bérces *et al.*²⁴ The reactivity of Nb_n with CO smoothly increases for $n \geq 3$ with no adsorbed products detected for $n=1$ and 2. The reaction with D₂ is observed as a function of cluster size. Nb₈, Nb₁₀, and Nb₁₆ are far less reactive than their neighbor Nb_n clusters in the reaction with D₂. Holmgren *et al.*²⁵ have studied the reaction of Nb_n with CO in a pickup cell experiment. The first CO adsorption probability exhibits a strong size dependence and

^{a)}Electronic mail: erb@lamar.colostate.edu.

Nb₁₀ shows very low reactivity with CO. Their results are different from those for a flow tube experiment in which no drop in reactivity of Nb₁₀ is observed. Reactions of V_{*n*} with CO and D₂ (separately) have also been studied in both flow tube²² and pickup¹⁹ cell experiments. Strong size dependent reactivity is observed with D₂ but not with CO. No reports are found for the reaction of Ta_{*n*} with CO and D₂/H₂, and only reactions with nitrogen, benzene, and aliphatic hydrocarbons are investigated for Ta_{*n*}.^{20,26–28}

Previous flow tube reactor studies^{21–23} suggest that H₂ is dissociatively adsorbed on M_{*n*} (M=V, Nb, ...), while CO is initially molecularly adsorbed on M_{*n*} clusters. Following initial molecular adsorption, CO can be dissociatively adsorbed on a metal cluster in an activated reaction by surmounting a reaction barrier. This chemistry is probably associated with the high CO bond strength [11.1 eV Ref. 29] and the cooling effect of buffer gas in a flow tube reactor. Thus, a cluster M_{*n*} can support and/or trap CO and facilitate a CO reaction with atomic hydrogen that is supposed to be active partly due to weak bonding between metal and hydrogen.²¹

Reactions of M_{*n*} (M=V and Nb) with CO and H₂ separately are widely investigated in the literature, but the reaction of metal clusters with mixed CO+H₂ has not been previously studied. In this report, we discuss, in particular, the reaction of CO+H₂ with metal clusters V_{*n*}, Nb_{*n*}, and Ta_{*n*} in a flow tube reactor. We suggest that the Nb₈ cluster is special in this group of metal clusters, in that Nb₈+CO+2H₂ → Nb₈CH₃OH. This finding is based on three observations: (1) The Nb₈CO(H₂)₂ cluster is the most abundant cluster for all Nb₈(CO)_{*x*}(H₂)_{*y*} (*x*=1, 2, and *y*=1, 2, 3, ...) clusters, independent of the concentration of H₂ for a given CO concentration. (2) Only Nb₈ and Nb₁₀ clusters do not completely dehydrogenate CH₃OH. (3) Nb₈COH₄/Nb₈CH₃OH is the only cluster that shows both dehydrogenation and a stable adsorbed species. These observations are supported by density functional theory (DFT) calculations of structures, frequencies, and reaction pathways.

II. PROCEDURES

A. Experimental

These experiments are carried out in both a flow tube reactor and a pickup cell. The pickup cell setup has been described previously,²⁰ and the design of our flow tube reactor is similar to the one adopted by Geusic *et al.*¹¹ A short summary of our flow tube experimental equipment is given below.

The vacuum system includes two vacuum chambers: the reaction chamber, which is for cluster generation and reaction, and the mass chamber, which is for detection of reactants and products. The two chambers are separated by a skimmer. The motivation for this two chamber design is to maintain a low pressure (10⁻⁶–10⁻⁷ Torr) in the mass chamber. M_{*n*} clusters are generated by laser ablation with a focused 532 nm laser (Nd³⁺:yttrium aluminum garnet, 10 Hz, 5–8 mJ/pulse, and 8 ns duration) onto a 12 mm diameter spring loaded metal disk [M=V (99.7%), Nb (99.8%), and Ta (99.99%), Sigma-Aldrich] in the presence of high purity (99.995%, Spectra Gas) pulsed helium carrier gas controlled

by a R. M. Jordan supersonic nozzle. A translational and rotational (spiral) motion of the disk is managed by a single motor (Maxon) that is powered by a homemade controller with a wide range of speed adjustment. Metal clusters are formed in an adjustable length gas channel with a “waiting room” upstream.¹⁵ Typical dimensions used in this system are 3 mm diameter by 5 mm length for the waiting room and 1.8 mm diameter by 44 mm length for the rest of the channel. The gas channel is coupled directly to a tube/reactor (stainless steel, 6.3 mm inner diameter by 76 mm length). The reactant gases, CO and H₂ (99.8% without further purification, General Air), and CH₃OH (99.9%, Sigma-Aldrich) are mixed with helium and injected into the reactor by a second pulsed valve (General Valve, series 9) with a pulse duration of about 1 ms. The delay time between the two valve openings is optimized to yield best product signals. Pressure in the flow tube reactor is estimated to be about 14 Torr in the presence of a reactant gas pulse. After reaction of M_{*n*} with CO+H₂ or CH₃OH in the reactor, reactants, products, and the buffer gases are expanded into the first chamber (~10⁻³–10⁻⁴ Torr) to form a molecular beam. The beam enters the vacuum of the second, detection mass spectrometer chamber (~10⁻⁶–10⁻⁷ Torr) through a 5 mm diameter skimmer. The clusters and products in the beam are ionized by a 193 nm excimer laser (10 mm by 2 mm rectangle, ~200 μJ/cm²). Ions are accelerated and detected by a time of flight mass spectrometer, and signals are recorded and averaged typically for 2500 laser shots by a digital storage oscilloscope (Tektronix TDS5032B).

B. Computational

Neutral, cationic, and anionic niobium clusters have been investigated by DFT calculations of their structures,^{30–33} binding energies,³⁰ and reaction pathways.^{34,35} In this study, calculations include geometry optimizations, vibrational frequency determination for the neutral Nb_{*n*} cluster, related Nb_{*n*}/CO/H₂ adsorption clusters, and the transition states of the reaction pathway. These DFT calculations are performed employing Becke’s exchange³⁶ and Perdew-Wang correlation³⁷ functional, denoted as BPW91, within the GAUSSIAN 03 package.³⁸ The LANL2DZ basis set, which involves the Los Alamos effective core potential plus a double zeta basis set, is employed to model the niobium atom, and the standard 6-311+G(2*d*,*p*) basis set has been used to model carbon, oxygen, and hydrogen atoms. All calculations are carried out with the GAUSSIAN 03 program.³⁸

III. RESULTS

A. Reactions of M_{*n*} with CO+H₂

Mass spectra for the neutral Nb_{*n*} cluster distribution (*n*=7–10), reactions of Nb_{*n*} clusters (*n*=7–10) with 50 ppm CO, 1.5% H₂, and 92 ppm CO+0.2% H₂ in a flow tube reactor are shown in Fig. 1. In Fig. 1(a), the mass spectrum of bare metal Nb_{*n*} (*n*=7–10) clusters is presented. Some carbide and oxide clusters are observed in the mass spectrum because carbon and oxygen impurities are difficult to remove in our experiments, even if high purity helium carrier gas

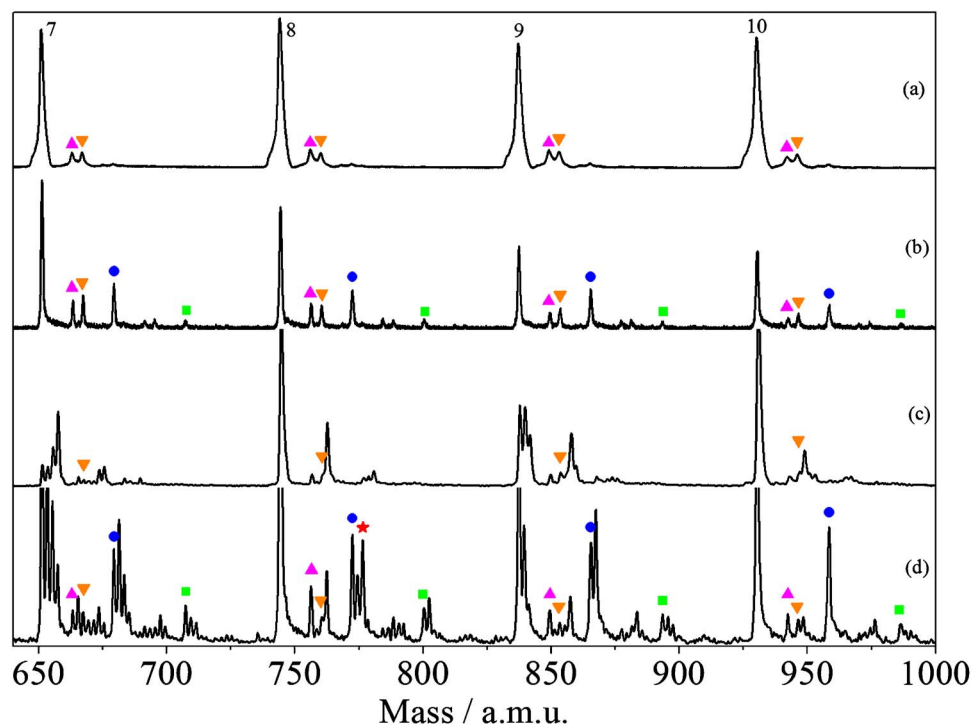


FIG. 1. (Color online) Product distribution for bare Nb_n ($n=7-10$) metal clusters (a), the reactions of Nb_n ($n=7-10$) with 50 ppm CO (b), 1.5% H₂ (c), and 92 ppm CO+0.2% H₂ (d) in a flow tube reactor. Ionization is by a 193 nm laser at a fluence of 200 $\mu\text{J}/\text{cm}^2$. \blacktriangle , \blacktriangledown , \bullet , \blacksquare , and \star indicate carbide impurities, oxide impurities, Nb_nCO, Nb_n(CO)₂, and Nb_nCOH₄, respectively. Note that hydrogen adsorbs on Nb_{7,9} clusters more readily than on Nb_{8,10}.

(99.995%) is employed for the expansion. For the reaction of Nb_n clusters with 50 ppm CO, primary and secondary adsorption products, Nb_nCO and Nb_n(CO)₂, are both detected for $n \geq 3$; only the $n=7-10$ cluster range is plotted in Fig. 1(b). With a 1.5% H₂/He gas mixture added to the flow tube reactor, one or more hydrogen molecules can adsorb on the Nb_n clusters for $n \geq 3$ and $n \neq 8$ and 10, as seen in Fig. 1(c). Nb₈ and Nb₁₀ are inert in the reaction with H₂ under these experimental conditions. Reaction of Nb_n clusters with a

mixture of CO and H₂ yields observed products Nb_nH_{2k} ($n \geq 3$ and $n \neq 8$ and 10, $k=1,2,3,\dots$) and Nb_nCOH_{2k} ($n \geq 3$ and $n \neq 10$, $k=1,2,3,\dots$), as shown in Fig. 1(d). Note that a relatively intense mass peak around the Nb₈ cluster is identified as Nb₈COH₄.

Mass spectra for the reaction of Nb_n ($n=7-10$) with 92 ppm CO+5%, 1%, and 0.2% H₂ are presented in Fig. 2. Nb₈COH₄ is always much stronger than its neighbor peaks Nb₈COH_{2k} ($k=1,3,4,\dots$) when H₂ concentration changes

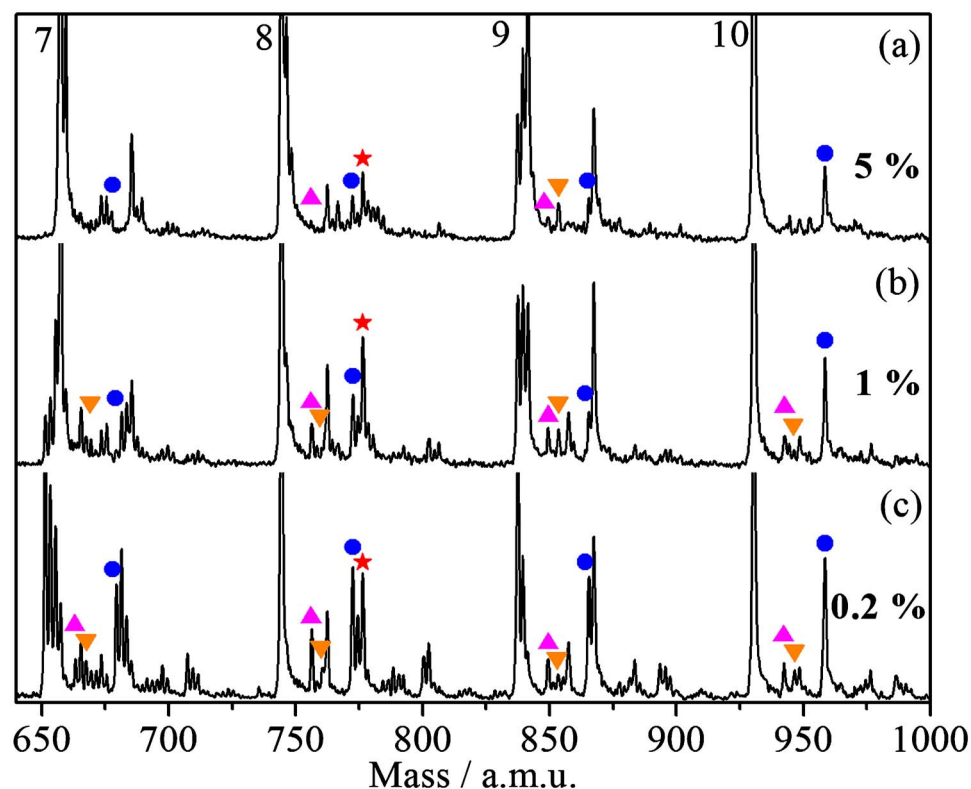


FIG. 2. (Color online) Product distribution for the reaction of Nb_n ($n=7-10$) with 92 ppm CO and 5% (a), 1% (b), and 0.2% (c) H₂ in a flow tube reactor. Ionization is by a 193 nm laser at a fluence of 200 $\mu\text{J}/\text{cm}^2$. \blacktriangle , \blacktriangledown , \bullet , and \star indicate carbide impurities, oxide impurities, Nb_nCO, and Nb₈COH₄, respectively. Note that the relative intensities of Nb₇COH_{2k} and Nb₉COH_{2k} ($k=1,2,3,\dots$) change as the hydrogen concentration is varied, while this is not the case for Nb₈COH_{2k}. Additionally, hydrogen adsorbs on Nb_{7,9} clusters more readily than on Nb_{8,10}.

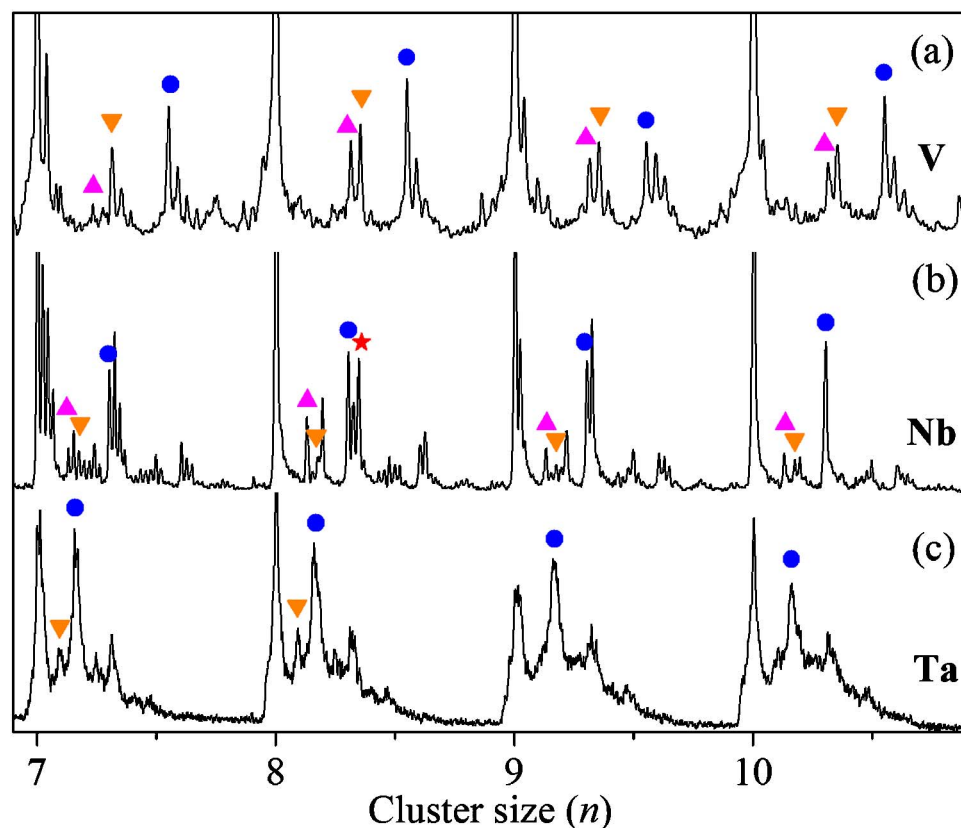


FIG. 3. (Color online) Product distribution for the reaction of V_n (a), Nb_n (b), and Ta_n (c) ($n=7-10$) with 92 ppm CO+0.2% H_2 in a flow tube reactor. Ionization is by a 193 nm laser at a fluence of $200 \mu J/cm^2$. ▲, ▼, ●, and ★ indicate carbide impurities, oxide impurities, M_nCO , and Nb_8COH_4 , respectively. Note the enhanced intensity for the Nb_8COH_4 feature in the mass spectra.

from 0.2% to 5%; however, other Nb_n ($n \geq 3$ and $n \neq 8$ and 10) clusters adsorb more hydrogen molecules as the hydrogen concentration is increased. For example, the strongest signal switches from Nb_7COH_2 to Nb_7COH_6 as the H_2 concentration is increased from 0.2% to 5%, as shown in Figs. 2(c) and 2(a). Because Nb_nCOH_4 has the same mass number as a Nb_nO_2 impurity, pure helium gas is injected in the flow tube reactor as a reference; the Nb_nO_2 signal contribution is negligible.

Mass spectra for the reaction of M_n ($M=V, Nb$, and Ta , $n=7-10$) clusters with 92 ppm CO+0.2% H_2 in a flow tube reactor are plotted in Fig. 3. Mass resolution for Ta_n clusters in Fig. 3(c) is reduced due to the high mass of Ta_n clusters (1267 amu for Ta_7 and 1810 amu for Ta_{10}) compared to that of V_n or Nb_n clusters. Hydrogen molecule adsorption products on M_n and M_nCO ($M=V$ and Ta , $n \geq 3$) clusters are observed, and $V_{8,10}$ clusters show low reactivity toward H_2 . For other clusters, no size dependent behavior is identified, as shown in Fig. 3. These observations are different from those for reaction of H_2 with Nb_n and Nb_nCO , presented in Fig. 1(d).

B. Reaction of M_n with CH_3OH

Product yields for M_n ($M=V, Nb$, and Ta) reacting with CH_3OH/He in a flow tube reactor are displayed in Fig. 4. Mass resolution in Fig. 4(c) is low due to the high mass of Ta_n clusters. In the reaction of Nb_n with CH_3OH , primary and secondary adsorption products are fully dehydrogenated to form Nb_nCO and $Nb_n(CO)_2$ for $n \geq 3$ and $n \neq 8$ and 10. For the Nb_{10} cluster, only nondehydrogenated products are detected as $Nb_{10}COH_4/Nb_{10}CH_3OH$ and

$Nb_{10}(COH_4)_2/Nb_{10}(CH_3OH)_2$ in our experiment. For the Nb_8 cluster, both nondehydrogenated products Nb_8COH_4/Nb_8CH_3OH and $Nb_8(CO)_2/Nb_8(CO)_2$ and fully dehydrogenated products Nb_8CO and $Nb_8(CO)_2$ are observed simultaneously in mass spectra shown in Fig. 4(b). Fully dehydrogenated products M_nCO and $M_n(CO)_2$ ($n=3-11$) are only identified in the reaction of V_n and Ta_n clusters with CH_3OH , as seen in Figs. 4(a) and 4(c). For the reaction of V_n , Nb_n , and Ta_n ($n=3-11$) clusters with CH_3OH , nondehydrogenated products are only observed for Nb_8 and Nb_{10} ; all other clusters in this study yield fully dehydrogenated product clusters.

C. Pickup cell experiments

Reactions of M_n ($M=V, Nb$, and Ta) with mixed gases CO+ H_2 in a pickup cell are also explored. Only CO adsorbed products M_nCO are observed for all the pickup cell experiments. Note that $Nb_{10}CO$ is relatively weaker than other Nb_nCO ($n \neq 10$) products, as observed by Holmgren *et al.*²⁵ M_nCO ($M=V, Nb$, and Ta) clusters are the only observed products for reactions of M_n with CH_3OH in the pickup cell. These species are fully dehydrogenated from M_nCH_3OH clusters. No product is detected for the Nb_{10} cluster.

IV. DISCUSSION

A. Reaction of Nb_n clusters with CH_3OH

Three types of reactions are identified for the interaction of Nb_n cluster with CH_3OH in the flow tube reactor experiments presented in Fig. 4(b). First, fully dehydrogenated

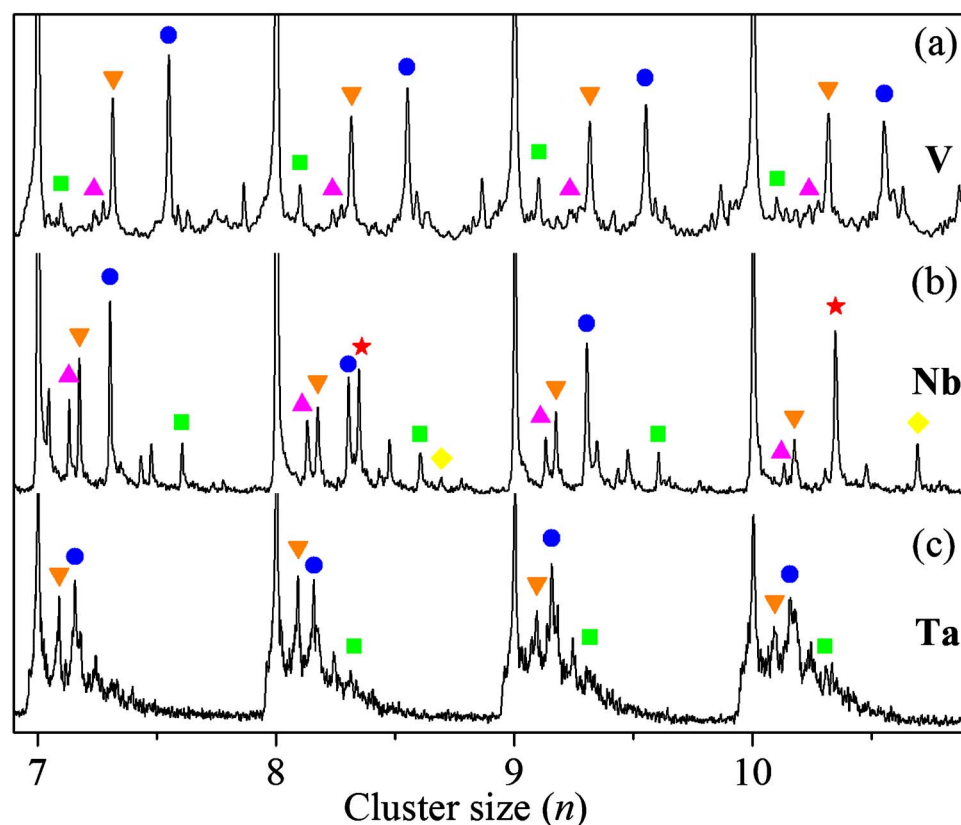


FIG. 4. (Color online) Product distribution for the reaction of V_n (a), Nb_n (b), and Ta_n (c) ($n=7-10$) with 55, 92, and 147 ppm CH_3OH in a flow tube reactor, respectively. Ionization is by a 193 nm laser at a fluence of $200 \mu J/cm^2$. \blacktriangle , \blacktriangledown , \bullet , \blacksquare , \blacklozenge , and \star indicate carbide impurities, oxide impurities, M_nCO , $M_n(CO)_2$, $Nb_n(CO)_2/Nb_n(CH_3OH)_2$, and Nb_nCO_4/Nb_nCH_3OH , respectively. Note that except for Nb_8 and Nb_{10} , CH_3OH is dehydrogenated on all the metal clusters.

products Nb_nCO are detected for $n \geq 3$ and $n \neq 8$ and 10. Second, for $n=10$, only the nondehydrogenated product $Nb_{10}CH_3OH/Nb_{10}COH_4$ is observed. Third, for $n=8$, both dehydrogenated and nondehydrogenated products are detected simultaneously, such as Nb_8CO/CNb_8O and Nb_8CH_3OH/Nb_8COH_4 . This size dependent behavior indicates the diverse dehydrogenation barriers existing for the reaction of Nb_n clusters with CH_3OH , as discussed below for these distinct cases:

- (1) For $n=3-11$ and $n \neq 8$ and 10, detection of fully dehydrogenated products indicates that the barrier for dehydrogenation of intermediate products Nb_nCH_3OH must be lower than the initial reactant energy of $Nb_n + CH_3OH$. In the flow tube reactor, Nb_n clusters generated from laser ablation are cooled to $\sim 300-400$ K due to a large number of collisions with the helium buffer gas. Therefore, if a high barrier exists for the CH_3OH dehydrogenation on Nb_n clusters, association products Nb_nCH_3OH should be observed in the mass spectrum [Fig. 4(b)]; however, only the fully dehydrogenated products Nb_nCO/CNb_nO are detected.
- (2) For $n=10$, instead of dehydrogenation products, only association products $Nb_{10}(CH_3OH)_{1,2}$ are observed, indicating that the dehydrogenation barriers for $Nb_{10}(CH_3OH)_{1,2}$ must be higher than the initial energy of $Nb_{10} + CH_3OH$. On the contrary, neither the association product $Nb_{10}CH_3OH$ nor the dehydrogenated product $Nb_{10}CO$ is observed in the pickup cell experiment. A similar behavior has been found for reaction of $Nb_{10} + CO$, in that the $Nb_{10}CO$ signal is significantly weaker than the other Nb_nCO ($n \neq 10$) signals in the

pickup cell experiment, but it is not weaker than the other cluster signals in the flow tube experiment.²⁵

These results illustrate that the binding energy between Nb_{10} and CO is weak and that cooling the $Nb_{10}CO$ association cluster in the flow tube reactor can help us to stabilize the weakly bound product: collisional cooling of intermediates does not occur in the pickup cell. Thus, a weakly bound molecular adsorption cluster between Nb_{10} and CH_3OH is similar to $Nb_{10}CO$ and can only occur in the flow tube reactor. Dehydrogenation of hydrocarbon compounds on transition metal surfaces must involve a hydrogen atom transfer to a metal atom.³⁵ Furthermore, a weakly bound association complex indicates a relatively long distance between the associated Nb_{10} and CH_3OH moieties and a relatively high barrier for hydrogen atom transfer from carbon and/or oxygen to niobium. Thus, only association products are observed for $Nb_{10} + CH_3OH$ in the flow tube experiment.

- (3) For $n=8$, two peaks, a dehydrogenated product Nb_8CO/CNb_8O and a nondehydrogenated product Nb_8CH_3OH/Nb_8COH_4 , are observed in the mass spectrum of $Nb_n + CH_3OH$, as shown in Fig. 4(b). One can estimate that the dehydrogenation barrier for Nb_8CH_3OH is close to the initial reactant energy of $Nb_8 + CH_3OH$. In the flow tube experiment, some Nb_8CH_3OH/Nb_8COH_4 intermediates are stabilized through collision with helium gas, and some can surmount the dehydrogenation barrier to produce Nb_8CO/CNb_8O . Consequently, the barrier height for dehydrogenation of CH_3OH on Nb_n clusters, from high

to low, is suggested to be $Nb_{10} > Nb_8 > Nb_n$ ($n \neq 8$ and 10).

B. Reaction of Nb_n clusters with $CO+H_2$

The stable species Nb_8CH_3OH/Nb_8COH_4 is observed as a product for the reaction of Nb_n clusters with $CO+H_2$. In the flow tube experiment, hydrogen association products Nb_8COH_{2k} ($k=1,2,3,\dots$) are observed, as shown in Fig. 1(d); however, hydrogen association products with bare metal clusters Nb_8H_{2k} ($k=1,2,3,\dots$) are not detected in either reaction with H_2 [Fig. 1(c)] or with mixture gases $CO+H_2$ [Fig. 1(d)]. Thus, CO adsorption on the Nb_8 surface prior to H_2 is suggested because adsorption of H_2 on a Nb_8 cluster has a relatively high barrier or a relatively low desorption energy.²³ The electronic structure of Nb_8 is changed by CO adsorption leading to a decrease of the hydrogen adsorption barrier (lower than the initial energy, Nb_8+CO+H_2). Therefore, Nb_8COH_{2k} species are observed in the mass spectrum of Fig. 1(d). An intense mass peak, Nb_8COH_4 , identified in the mass spectra in Figs. 1(d) and 2, is always stronger than its neighbor mass peaks Nb_8COH_2 and Nb_8COH_6 under the condition of different hydrogen concentrations in the flow tube reactor. This behavior is different from that of other Nb_n clusters. For $n=10$, neither hydrogen association products $Nb_{10}H_{2k}$ nor $Nb_{10}COH_{2k}$ are observed due to a weak bond between hydrogen molecules and Nb_{10} and $Nb_{10}CO$ or a high adsorption barrier as above for Nb_8 . The pickup cell experiment²⁵ suggests that the binding energy of Nb_{10} with CO is low and thereby, the chemical behavior of Nb_{10} and $Nb_{10}CO$ toward adsorption of H_2 can be expected to be similar. Thus, no H_2 adsorption on Nb_{10} and $Nb_{10}CO$ is observed, as shown in Figs. 1(d) and 2. For $n \geq 3$ and $n \neq 8$ and 10, one or more hydrogen association products Nb_nCOH_{2k} ($k=1,2,3,\dots$) are observed in our flow tube experiments, as shown in Fig. 1(d), and mass peak intensities of hydrogen rich clusters decrease with the number of adsorbed hydrogen molecules, e.g., $Nb_7COH_2 > Nb_7COH_4 > Nb_7COH_6$. This observation indicates that hydrogen adsorption is controlled by a kinetic process; this process is also confirmed by the change of Nb_nCOH_{2k} relative intensity with change in CO/H_2 concentration (see Fig. 2). For example, Nb_7COH_2 is the most intense mass peak for low (0.2%) hydrogen concentration, while Nb_7COH_6 is the most intense peak for high (5%) hydrogen concentration in the flow tube reactor. Thus, Nb_8COH_4 is a stable structure, and its formation is controlled by dynamic energetic processes (temperature, barrier, electronic structure,...) rather than by adsorption kinetics. This result is strongly supported by the results of the Nb_n cluster reactions with CH_3OH , as discussed above.

The product Nb_8COH_4 is observed in mass spectra for the reaction of Nb_8 with $CO+H_2$, but the structure of Nb_8COH_4 cannot be directly identified. Nb_8COH_4 has several possible structures: (1) CH_3OH adsorbed on Nb_8 , (2) CO molecularly adsorbed on Nb_8 with four hydrogen atoms dissociatively adsorbed on Nb_8 , (3) both CO and four hydrogen atoms dissociatively adsorbed on Nb_8 , (4) CO dissociatively adsorbed on Nb_8 and four hydrogen atoms dissociatively

adsorbed on CO ligand, and other possibilities. Infrared spectroscopy to detect C–H and/or O–H vibrations of Nb_8COH_4/Nb_8CH_3OH would be a useful method to explore product structure. Unfortunately, infrared multiphoton dissociation experiments do not produce a change in the appropriate mass channels due to very weak signals and/or cross section issues, and $Nb_8CH_3OH(Ar)_n$ neutral clusters apparently do not form in our experiments because these clusters are too hot for weak van der Waals bonds to form and stabilize.

C. Mechanism of methanol formation on Nb_8 cluster: DFT calculations

The observation of a stable Nb_8COH_4 product in both reactions of Nb_8+CO+H_2 and Nb_8+CH_3OH suggests that CH_3OH can be generated on Nb_8 by the following reaction ($\Delta H=-1.05$ eV based on DFT calculations) presented below and in Fig. 5:



DFT calculations are performed at the BPW91/LANL2DZ/6-311+G(2d,p) level to explore the possibility of CH_3OH formation on a Nb_8 cluster through reaction (2). In these DFT calculations, the lowest spin states of all calculated structures of the Nb_8 cluster and intermediates are singlets. To have an idea of the validity of the adopted DFT method and basis function, Table I summarizes some calculated and available experimental adiabatic ionization energies of Nb_n and related clusters Nb_nCO/CNb_nO ($n=3$ and 8). The adiabatic ionization energies for Nb_3 and Nb_8 clusters are 5.88 and 5.35 eV, which are in good agreement with experimental data of 5.81 and 5.48 eV,³⁹ respectively. Our calculational results are better than those obtained at the B3P86/LANL2DZ level.³⁴ For the dissociatively adsorbed CO cluster CNb_3O , the ionization energy is predicted to be 6.03 eV, also in agreement with 5.82(± 0.02) eV as measured by photoionization efficiency spectroscopy.³⁴ The calculated binding energies of CO with Nb_3 are larger by 0.64–0.90 eV at the B3P86/LANL2DZ level than those at the BPW91/LANL2DZ/6-311+G(2d) level, as listed in the last column of Table I.

The potential energy surface profile for CH_3OH formation from $CO+H_2$ on neutral Nb_8 clusters is shown in Fig. 5. The structures of intermediates and transition states on this surface are schematically shown in Fig. 6. The minima connected by a given transition state are confirmed by intrinsic reaction coordinate calculations as manipulated in the GAUSSIAN 03 program. As shown in Fig. 5, the first step, molecular adsorption of CO on the Nb_8 cluster to form Nb_8CO , is an exothermic reaction. Via transition state TS0, the molecular adsorption product Nb_8CO can transform to a dissociative adsorption product CNb_8O (shown by the dash line in Fig. 5). Thus, dissociative adsorption or molecular adsorption strongly depends on the details of the metals and adsorbed molecules.^{34,40} A H_2 adsorption channel for dissociation of one hydrogen molecule on Nb_8 and formation of $Nb_8HH(CO)$ is available, and a more favorable pathway with H_2 molecules is present in the reaction. Therefore, dis-

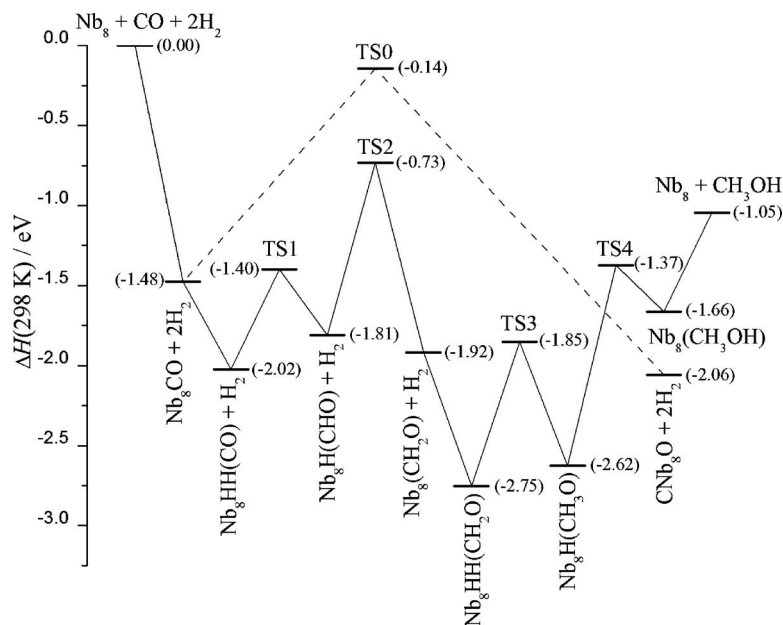


FIG. 5. A potential energy surface profile for the reaction $\text{Nb}_8 + \text{CO} + 2\text{H}_2 \rightarrow \text{Nb}_8 + \text{CH}_3\text{OH}$. Energies are in eV and relative to the initial reactant energy of $\text{Nb}_8 + \text{CO} + 2\text{H}_2$. Energy levels are calculated by BPW91/LANL2DZ/6-311+G(2d,p). See text for details.

sociative adsorption of CO on Nb₈ cluster will be inhibited for the reaction of Nb₈ with CO+H₂.

Molecular adsorption of CO on the Nb₈ cluster allows CH₃OH to be formed on Nb₈ through reaction with CO + 2H₂, as illustrated by the solid lines connecting transition states TS_x ($x=1, 2, 3$, and 4) and reaction intermediates in Fig. 5. After molecular adsorption of CO, one hydrogen molecule is first dissociatively adsorbed on Nb₈CO forming Nb₈HH(CO). These two hydrogen atoms transfer from the Nb₈ moiety to the CO ligand, one by one, by surmounting transition states TS1 and TS2, and Nb₈(CH₂O) is formed. Subsequently, another adsorbed hydrogen molecule is dissociated on the Nb₈(CH₂O) cluster, and one hydrogen atom transfers to the CO ligand and another one still stays on the Nb₈ moiety. A stable intermediate Nb₈HH(CH₂O) (2.75 eV lower than the initial energy) is formed, as shown in Figs. 5 and 6. The transfer of the last H atom leads to Nb₈(CH₃OH) via TS4 and finally generates product Nb₈+CH₃OH. Based on DFT calculations, the overall reaction of $\text{Nb}_8 + \text{CO} + 2\text{H}_2 \rightarrow \text{Nb}_8 + \text{CH}_3\text{OH}$ is barrierless and thermodynamically favorable. Free CH₃OH molecules cannot be detected by single photon ionization from a 193 nm laser—the ionization energy of CH₃OH is ~ 10.84 eV.⁴¹

The key step for methanol formation on neutral Nb₈

clusters is that CO must be molecularly adsorbed on the Nb₈ cluster surface. If CO were to dissociate rapidly on the clusters to form CNb_nO before collision with hydrogen molecules, recombination of carbon and oxygen atoms would not be possible, and transfer of hydrogen atoms to form methanol could not occur. Thus, the CO dissociation rate constant on the clusters is an essential parameter for the formation of methanol. According to Rice-Ramsberger-Kassel-Markus (RRKM) theory, the dissociation reaction rate constant for $\text{Nb}_n\text{CO} \rightarrow \text{CNb}_n\text{O}$ is given by

$$k_{\text{dis}} = \nu(1 - E_0/E)^{S-1},$$

in which ν is the effective frequency of the Nb_nCO dissociation coordinate vibration ($\nu=3 \times 10^{12} \text{ s}^{-1}$, $\sim 100 \text{ cm}^{-1}$ is assumed), S (intermolecular degrees of freedom) $=3n-6$, E_0 is the activation energy, E is the total energy $E=E_a+E_k+E_v$, E_a is the association energy given by $E(\text{Nb}_n\text{CO}) - (E(\text{Nb}_n) + E(\text{CO}))$, E_k is the center of mass kinetic energy (~ 0.3 eV), and E_v is the vibrational energy, given by $(3n-6)kT_v$. A vibrational temperature of 350 K (reasonable for the flow tube reactor) is assumed. For Nb₈ cluster, $E_0 = 1.48 - 0.14 = 1.34$ eV and $E = 1.48 + 0.3 + 0.72 = 2.50$ eV, as shown in Fig. 5. Based on the RRKM calculation, the reaction rate constant $k_8 = 6.41 \times 10^4 \text{ s}^{-1}$, and the lifetime of the transition state ($t_8 = 1/k_8$) is around 15.6 μs . These results indicate that CO remains molecularly adsorbed on Nb₈ cluster surface and the intermediate Nb₈CO can undergo many collisions with hydrogen molecules before CO dissociates on the cluster. Consequently, hydrogen molecules are adsorbed and a potential reaction pathway for methanol formation is displayed in Fig. 5.

The CO dissociation rate constants on Nb₃, Nb₄, and Nb₇ are likewise calculated as 3.18×10^{10} , 3.71×10^8 , and $5.41 \times 10^7 \text{ s}^{-1}$, respectively, as listed in Table II. Note that the rate constants k_3 , k_4 , and k_7 are much larger than k_8 , which suggests that CO is rapidly dissociated (within nanoseconds) to CNb_nO on the Nb_n clusters ($n=3, 4$, and 7) prior to collision with H₂/He. Thus, methanol formation is suppressed

TABLE I. Adiabatic ionization energies (IEs) and binding energies of neutral Nb₃, Nb₃CO, CNb₃O, Nb₈, Nb₈CO, and CNb₈O, as calculated by BPW91/LANL2DZ/6-311+G(2d).

Clusters	Calc. IE (eV)	Expt. IE (eV)	Binding energy (eV)
Nb ₃	5.88/6.8 ^a	5.81 ^b	...
Nb ₃ CO	5.46/6.6 ^a	...	1.96/2.60 ^a
CNb ₃ O	6.03/6.8 ^a	5.82 ^a	2.89/3.79 ^a
Nb ₈	5.35	5.48 ^b	...
Nb ₈ CO	5.26	...	1.45
CNb ₈ O	5.34	...	2.28

^aReference 34.

^bReference 39.

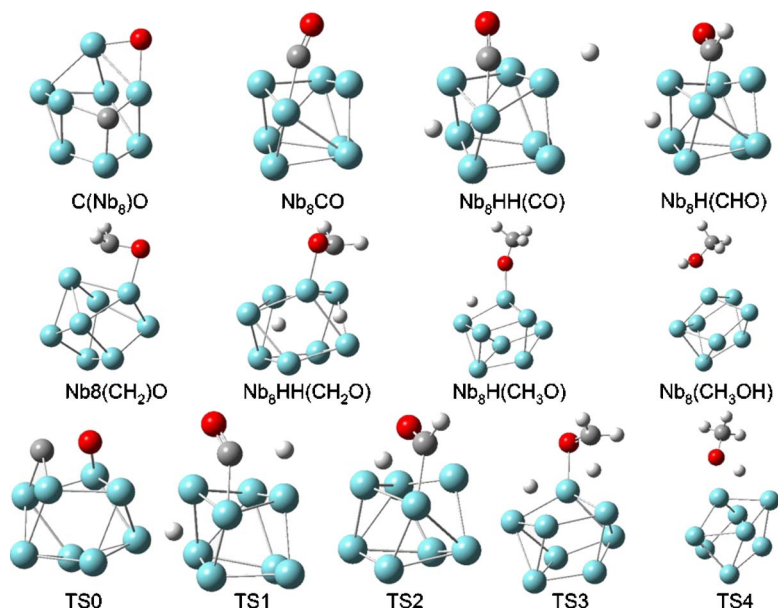


FIG. 6. (Color online) Structures of the reaction intermediates and transition states, as shown in Fig. 5. Niobium, oxygen, carbon, and hydrogen atoms are colored in light blue, red, gray, and light gray, respectively, on-line. In the print version, niobium atoms are large size and light gray, oxygen atoms are medium size and dark gray, carbon atoms are medium size and gray, and hydrogen atoms are small and lighter gray.

on Nb_n ($n \neq 8$) cluster surfaces as CO can dissociate on these clusters before the Nb_nCO intermediate can adsorb a hydrogen molecule. In addition, as seen from Table II, the association energy of $Nb_{10}CO$ is estimated at 1.23 eV (lower than for other clusters), and the $Nb_{10}CO$ bond is the weakest of all those calculated. This trend is in good agreement with the literature^{25,30} and our experimental results.

While proving a negative, that is, that Nb_n ($n \neq 8$) does not support the reaction $CO+2H_2 \rightarrow CH_3OH$, is notoriously difficult, the above calculations and discussion point out that the path chosen for Nb_8 to generate methanol from CO and H_2 is not readily available to clusters of similar size ($n=3-10$ and $n \neq 8$).

Additionally, no obvious systematic, size dependent behavior is observed for the reactions of M_n ($M=V$ and Ta) with $CO+H_2$ and CH_3OH . For reactions of V_n and Ta_n clusters with CH_3OH , all adsorbed products are fully dehydrogenated; this means that the dehydrogenation barriers for such reactions are lower than the initial energies for M_n+CH_3OH . No special mass peak for M_nCOH_4 ($M=V$ and Ta) is observed for reactions of V_n and Ta_n clusters with $CO+H_2$, either in the flow tube reactor or pickup cell. As can be surmised from Fig. 5, other metal clusters ($M_n=V_n, Nb_n$, and Ta_n , but $M_n \neq Nb_8$) do not form CH_3OH in such a reac-

tion because the hydrogen transfer barriers for M_nCO are probably too high. Additionally, if the hydrogen transfer barriers are relatively low and some CH_3OH is formed on M_n clusters, M_nCH_3OH should readily dehydrogenate to M_nCO/CM_nO due to the low dehydrogenation barriers.

V. CONCLUSIONS

Reaction of CO with H_2 on neutral V_n , Nb_n , and Ta_n clusters in the gas phase is explored by employing a flow tube reactor and a time of flight mass spectrometer with 193 nm single photon ionization. A strong size dependent reactivity of Nb_n toward CO, H_2 , and CH_3OH is characterized. A stable product Nb_8COH_4 is identified for reactions of both Nb_n+CO+H_2 and Nb_n+CH_3OH , which suggests that CH_3OH is formed on the Nb_8 cluster through reaction of $Nb_8+CO+2H_2$. Furthermore, theoretical DFT calculations indicate that the reaction of $Nb_8+CO+2H_2 \rightarrow Nb_8+CH_3OH$ is barrierless and thermodynamically and kinetically favorable. According to our DFT calculations, stable structures are formed for $Nb_8HH(CH_2O)$, $Nb_8H(CH_3O)$, and $Nb_8(CH_3OH)$ species on the reaction potential energy surface. For all other V_n , Nb_n ($n \neq 8$), and Ta_n clusters, either the hydrogen transfer barrier is high so that CH_3OH formation does not occur or the hydrogen transfer barrier is low enough so that CH_3OH is formed, but it is not preserved on the clusters due to a low dehydrogenation barrier.

ACKNOWLEDGMENTS

This work was supported by the U.S. DOE BES Program and the NSF ERC for Extreme Ultraviolet Science and Technology under NSF Award No. 0310717.

¹X. M. Liu, G. Q. Lu, Z. F. Yan, and J. Beltramini, Ind. Eng. Chem. Res. **42**, 6518 (2003).

²S. Wasmus and A. Küver, J. Electroanal. Chem. **461**, 14 (1999).

³L. Carrette, K. A. Friedrich, and U. Stimming, ChemPhysChem **1**, 162 (2000).

⁴M. Xu, J. H. Lunsford, D. W. Goodman, and A. Bhattacharyya, Appl. Catal., A **149**, 289 (1997).

TABLE II. CO dissociation barriers and reaction rate constants on Nb_n cluster surface, as calculated by BPW91/LANL2DZ/6-311+G(2d). Energies are in eV and relative to the initial energy (Nb_n+CO).

Clusters	Nb_nCO^a	TS0 ^b	k_n (s ⁻¹) ^c	t_n (s) ^d
Nb_3	1.99	0.88	3.18×10^{10}	3.15×10^{-11}
Nb_4	1.81	0.43	3.71×10^8	2.70×10^{-9}
Nb_7	1.66	0.57	5.41×10^7	1.85×10^{-8}
Nb_8	1.48	0.14	6.41×10^4	1.56×10^{-5}
Nb_{10}	1.23

^aAssociation energy.

^bTransition state energy for Nb_nCO to CNb_nO .

^cCalculated reaction rate constant.

^dTransition state lifetime $t_n=1/k_n$.

- ⁵N. D. Parkyns, C. I. Warburton, and J. D. Wilson, *Catal. Today* **18**, 385 (1993).
- ⁶F. A. P. Cavalcanti, A. Y. Stakheev, and W. M. H. Sachtler, *J. Catal.* **134**, 226 (1992).
- ⁷D. K. Bohme and H. Schwarz, *Angew. Chem., Int. Ed.* **44**, 2336 (2005).
- ⁸O. P. Balaj, I. Balteanu, T. T. J. Roteuscher, M. K. Beyer, and V. E. Bondybey, *Angew. Chem., Int. Ed.* **43**, 6519 (2004).
- ⁹R. A. J. O'Hair and G. N. Khairallah, *J. Cluster Sci.* **15**, 331 (2004).
- ¹⁰D. E. Powers, S. G. Hansen, M. E. Geusic, A. C. Puiu, J. B. Hopkins, T. G. Dietz, M. A. Duncan, P. R. R. Langridge-Smith, and R. E. Smalley, *J. Phys. Chem.* **86**, 2556 (1982).
- ¹¹M. E. Geusic, M. D. Morse, S. C. O'Brien, and R. E. Smalley, *Rev. Sci. Instrum.* **56**, 2123 (1985).
- ¹²R. L. Whetten, D. M. Cox, D. J. Trevor, and A. Kaldor, *J. Phys. Chem.* **89**, 566 (1985).
- ¹³R. J. S. Pierre and M. A. El-Sayed, *J. Phys. Chem.* **91**, 763 (1987).
- ¹⁴R. J. S. Pierre, E. L. Chronister, and M. A. El-Sayed, *J. Phys. Chem.* **91**, 5228 (1987).
- ¹⁵M. Andersson, J. L. Persson, and A. Rosén, *J. Phys. Chem.* **100**, 12222 (1996).
- ¹⁶M. Andersson and A. Rosén, *J. Chem. Phys.* **117**, 7051 (2002).
- ¹⁷L. Holmgren, M. Andersson, and A. Rosén, *Chem. Phys. Lett.* **296**, 167 (1998).
- ¹⁸L. Holmgren, M. Andersson, and A. Rosén, *J. Chem. Phys.* **109**, 3232 (1998).
- ¹⁹L. Holmgren and A. Rosén, *J. Chem. Phys.* **110**, 2629 (1999).
- ²⁰S.-G. He, Y. Xie, F. Dong, and E. R. Bernstein, *J. Chem. Phys.* **125**, 164306 (2006).
- ²¹M. D. Morse, M. E. Geusic, J. R. Heath, and R. E. Smalley, *J. Chem. Phys.* **83**, 2293 (1985).
- ²²D. M. Cox, K. C. Reichmann, D. J. Trevor, and A. Kaldor, *J. Chem. Phys.* **88**, 111 (1988).
- ²³M. R. Zakin, R. O. Brickman, D. M. Cox, and A. Kaldor, *J. Chem. Phys.* **88**, 3555 (1988).
- ²⁴A. Bérces, P. A. Hackett, L. Lian, S. A. Mitchell, and D. M. Rayner, *J. Chem. Phys.* **108**, 5476 (1998).
- ²⁵L. Holmgren, M. Andersson, and A. Rosén, *Surf. Sci.* **331–333**, 231 (1995).
- ²⁶Y. M. Hamrick and M. D. Morse, *J. Phys. Chem.* **93**, 6494 (1989).
- ²⁷J. T. Lyon and L. Andrews, *J. Phys. Chem. A* **109**, 431 (2005).
- ²⁸D. B. Pedersen, J. M. Parnis, R. D. Lafleur, and D. M. Rayner, *J. Phys. Chem. A* **108**, 2682 (2004).
- ²⁹K. P. Huber and G. Herzberg, *Constants of Diatomic Molecules* (Van Nostrand Reinhold, New York, 1979).
- ³⁰H. Grönbeck and A. Rosén, *Phys. Rev. B* **54**, 1549 (1996).
- ³¹L. Goodwin and D. R. Salahub, *Phys. Rev. A* **47**, R774 (1993).
- ³²R. Fournier, T. Pang, and C. Chen, *Phys. Rev. A* **57**, 3683 (1998).
- ³³H. Grönbeck, A. Rosén, and W. Andreoni, *Phys. Rev. A* **58**, 4630 (1998).
- ³⁴D. B. Pedersen, D. M. Rayner, B. Simard, M. A. Addicoat, M. A. Buntine, G. F. Metha, and A. Fielicke, *J. Phys. Chem. A* **108**, 964 (2004).
- ³⁵I. Rivalta, N. Russo, and E. Sicilia, *J. Mol. Struct.: THEOCHEM* **762**, 25 (2006).
- ³⁶A. D. Becke, *Phys. Rev. A* **38**, 3098 (1988).
- ³⁷J. P. Perdew and Y. Wang, *Phys. Rev. B* **45**, 13244 (1991).
- ³⁸M. J. Frisch, G. W. Trucks, H. B. Schlegel *et al.*, GAUSSIAN 03, revision C.02, Gaussian, Inc., Wallingford, CT, 2004.
- ³⁹M. B. Knickelbein and S. Yang, *J. Chem. Phys.* **93**, 5760 (1990).
- ⁴⁰A. Fielicke, G. von Helden, G. Meijer, D. B. Pedersen, B. Simard, and D. M. Rayner, *J. Chem. Phys.* **124**, 194305 (2006).
- ⁴¹K. Watanabe, *J. Chem. Phys.* **26**, 542 (1957).